A discontinuous Galerkin FEM multi-physics solver for the molten salt fast reactor

Tiberga, Marco; Lathouwers, Danny; Kloosterman, Jan Leen

Publication date
2019

Document Version
Accepted author manuscript

Published in
International Conference on Mathematics and Computational Methods Applied to Nuclear Science and Engineering, M and C 2019

Citation (APA)
Tiberga, M., Lathouwers, D., & Kloosterman, J. L. (2019). A discontinuous Galerkin FEM multi-physics solver for the molten salt fast reactor. In J. Wagner, & J. Rathkopf (Eds.), *International Conference on Mathematics and Computational Methods Applied to Nuclear Science and Engineering, M and C 2019* (pp. 1818-1827). (International Conference on Mathematics and Computational Methods Applied to Nuclear Science and Engineering, M and C 2019). American Nuclear Society.

Important note
To cite this publication, please use the final published version (if applicable).
Please check the document version above.

A DISCONTINUOUS GALERKIN FEM MULTI-PHYSICS SOLVER FOR THE MOLTEN SALT FAST REACTOR

Marco Tiberga[1], **Danny Lathouwers**[1], **and Jan Leen Kloosterman**[1]
[1]Department of Radiation Science and Technology
Delft University of Technology
Mekelweg 15, 2629 JB Delft, The Netherlands
M.Tiberga@tudelft.nl; D.Lathouwers@tudelft.nl; J.L.Kloosterman@tudelft.nl

ABSTRACT

Numerical simulations of fast MSRs constitute a challenging task. In fact, classical codes employed in reactor physics cannot be used, and new dedicated multi-physics tools must be developed, to capture the unique features of these systems: the strong coupling between neutronics and thermal-hydraulics due to the use of a liquid fuel, the effects on reactor kinetics induced by the precursors drift, the internal heat generation, and the shape of the core having no fuel pins as a repeated structure. In this work, we present a novel multi-physics tool being developed at TU Delft. The coupling is realized between an S_N radiation transport code (`PHANTOM-`S_N) and a RANS solver (`DGFlows`). Both in-house tools are based on a Discontinuous Galerkin Finite Element space discretization, characterized by local conservation, high-order accuracy, and allowing for high geometric flexibility. Implicit discretization in time is performed adopting Backward Differentiation Formulae. Cross sections are computed on an element base, starting from the local average temperature and a set of libraries generated at reference temperatures with Monte Carlo or deterministic codes. Comparison of the results obtained performing a suitable numerical benchmark created at LPSC/CNRS/Grenoble with those available in literature shows that the multi-physics tool is able to capture the unique phenomena characterizing fast liquid-fueled systems.

KEYWORDS: Multi-physics, MSFR, Discontinuous Galerkin FEM, S_N transport.

1. INTRODUCTION

Research on liquid-fueled reactors has regained momentum in the last decade, especially after the Molten Salt Fast Reactor (MSFR) was included in the scope of Generation IV nuclear reactors [1]. Its characteristics make it a promising option, in terms of safety, reliability, and sustainability [2], to help meet the world's rising energy needs and, at the same time, to try to obtain the support of public opinion always concerned about waste storage, proliferation, and safety. In Europe, research efforts are currently coordinated by the H2020 SAMOFAR project (http://samofar.eu/), whose main goal is to prove the innovative safety aspects of the MSFR design, during operational and accidental transient scenarios, by advanced experimental and numerical techniques.

Simulating fast MSRs is a challenging task, as the employed multi-physics tools must be able to capture the unique features of these systems, stemming from the use of a molten salt that is both

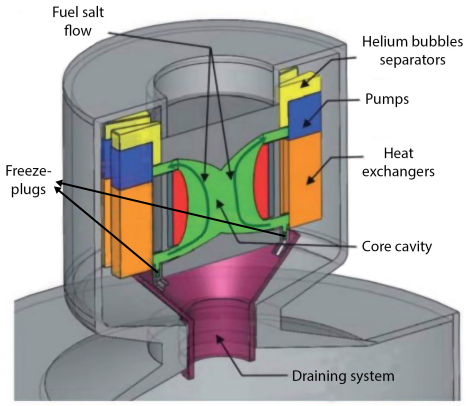

Figure 1: Layout of MSFR fuel circuit and draining system.

fuel and coolant: strong coupling between neutronics and thermal-hydraulics; internal heat generation in the fluid; and transport of delayed neutron precursors, which affects the multiplication factor and reduces the margin to prompt criticality. Moreover, the traditional shape of the core with fuel pins as a repeated structure is lost, replaced by complex geometries (see Figure 1, for a schematic view of the MSFR toroidal fuel circuit). Classical codes used in reactor physics are, therefore, unsuitable for simulating the MSFR behavior, and new dedicated tools must be developed (e.g., [3–6]).

In this work, we present a novel multi-physics tool being developed at Delft University of Technology. The coupling is realized between a CFD code named `DGFlows` and a radiation transport code named `PHANTOM-`S_N. Both in-house tools are based on a Discontinuous Galerkin Finite Element (DG-FEM) space discretization, which combines the advantages of local conservation, as in finite volumes, with the high-order discretization and high geometric flexibility (thus easily handling complex shapes as the MSFR core) of finite elements, guaranteeing high accuracy of simulations. Details about the model equations as well as their space-time discretization and about the coupling scheme are provided in Section 2. In Section 3, we compare the results obtained performing a suitable numerical benchmark created at LPSC/CNRS/Grenoble with those available in literature, in order to assess the capabilities of the multi-physics tool to capture the unique phenomena characterizing the MSFR.

2. DESCRIPTION OF THE MULTI-PHYSICS TOOL

2.1. Thermal-hydraulics: `DGFlows` Code

`DGFlows` solves the set of compressible Navier-Stokes equations, in the low-Mach limit approximation. Turbulent flows are handled through Reynolds Averaged Navier-Stokes (RANS) models. The model equations read (omitting dependencies for clarity)

$$\frac{\partial \rho h}{\partial t} + \nabla \cdot (\mathbf{u} \rho h) = -\nabla \cdot \mathbf{q} + S_h, \tag{1}$$

$$\frac{\partial \rho \mathbf{u}}{\partial t} + \nabla \cdot (\mathbf{u} \rho \mathbf{u}) = -\nabla p + \nabla \cdot \tau + \mathbf{S}_{\mathbf{u}}, \tag{2}$$

$$\frac{\partial \rho}{\partial t} + \nabla \cdot (\mathbf{u} \rho) = 0, \tag{3}$$

where ρ is the density, $\mathbf{u}$ the velocity, p the pressure, and h the specific enthalpy. The heat flux $\mathbf{q}$ and the Newtonian shear stress tensor τ are respectively defined as

$$\mathbf{q} = -\lambda_{eff} \nabla T, \tag{4}$$

$$\tau = \mu_{eff} \left[\nabla \mathbf{u} + (\nabla \mathbf{u})^T - \frac{2}{3} (\nabla \cdot \mathbf{u}) I \right], \tag{5}$$

where I is the identity tensor, while μ_{eff} and λ_{eff} are the effective dynamic viscosity and heat conductivity; they reduce to the molecular ones for laminar flows. `DGFlows` can handle material properties fully-variable with temperature. Finally, $\mathbf{S}_{\mathbf{u}}$ and S_h are the sources of momentum and energy (e.g., buoyancy, fission heat). In MSRs simulations, the Boussinesq approximation can often be adopted for buoyancy, thus reducing Eq. (3) to the standard divergence-free constraint on the velocity field for incompressible flows.

System (1)–(3) is closed with the standard RANS models $k - \epsilon$ or $k - \omega$ and with a set of proper initial and boundary conditions. In this work, we consider flows bounded by adiabatic walls; when laminar, they require the imposition of the following conditions (introducing $\mathbf{n}$ as the outward normal to the boundary surface): no penetration ($\mathbf{n} \cdot \mathbf{u} = \mathbf{0}$), no slip ($\mathbf{u} = \mathbf{u}_D$), and no-heat-flux ($\mathbf{n} \cdot \mathbf{q} = 0$); when turbulent flows are simulated, the standard logarithmic wall-functions are imposed.

2.1.1. Spatial discretization

Spatial discretization is performed using the Discontinuous Galerkin FEM approach, adopting a hierarchical set of modal basis functions up to order $\mathcal{P}$. The discretization closely follows what described by Shahbazi et al. [7], so we report only the key ingredients here, omitting details.

Diffusive terms are discretized with the Symmetric Interior Penalty (SIP) method, which is consistent and stable and leads to optimal space error convergence rates and compact stencils size. Differently from [7], we solve for the set of conservative variables to fully exploit the local conservation of DG; consequently, we need to modify diffusion terms like (4) and (5), expressed in terms of primitive variables, and to use a generalized form of the SIP method. For example, the discretization of the viscous term in the momentum equation results into the following bilinear and RHS operators:

$$\begin{aligned} b^{\mathrm{gSIP}}(\mathbf{m}, \mathbf{v}) = & \sum_{E \in \mathcal{E}_h} \int_E \tau(\mathbf{m}) \colon \nabla \mathbf{v} + \sum_{F \in \mathcal{F}_h^{\mathrm{i,D}}} \int_F \eta_F \, [\![\mathbf{m}]\!] \, [\![\mathbf{v}]\!] + \\ & - \sum_{F \in \mathcal{F}_h^{\mathrm{i,D}}} \int_F \mathbf{n}_F \cdot \left(\{\tau(\mathbf{m})\} \cdot [\![\mathbf{v}]\!] + \{\tau(\mathbf{v})\} \cdot [\![\mathbf{m}]\!] \right), \end{aligned} \tag{6}$$

$$l^{\mathrm{gSIP}}(\mathbf{v}) = \sum_{F \in \mathcal{F}_h^{\mathrm{D}}} \left(\eta_F \, \mathbf{u}_{\mathrm{D}} \cdot \mathbf{v} - \mathbf{u}_{\mathrm{D}} \cdot \tau(\mathbf{v}) \cdot \mathbf{n}_F \right). \tag{7}$$

Here, $\mathcal{E}_h$ is the set of mesh elements, while $\mathcal{F}_h^{\mathrm{i}}$ and $\mathcal{F}_h^{\mathrm{D}}$ are the sets of internal and Dirichlet boundary faces respectively; $\mathbf{m}$ is the mass flux, $\mathbf{v}$ the test function, while η_F is a sufficiently high penalty parameter; $[\![\cdot]\!]$ and $\{\cdot\}$ denote the jump and average operators, defined as $[\![\mathbf{v}]\!] = \mathbf{v}_1 - \mathbf{v}_2$ and $\{\mathbf{v}\} = 0.5(\mathbf{v}_1 + \mathbf{v}_2)$, where the subscripts indicate the values of the function on the two face sides. Finally, $\mathbf{n}_F$ is the face normal. The diffusion term in the enthalpy equation leads to a null RHS term, given the (natural) no-heat-flux boundary condition applied at walls.

Convective terms are discretized with the Lax-Friedrichs numerical flux. Taking again the momentum equation as example, we get the following trilinear form:

$$b^{\mathrm{LF}}(\mathbf{u}^*, \mathbf{m}, \mathbf{v}) = -\sum_{E \in \mathcal{E}_h} \int_E \mathbf{v} \cdot (\mathbf{u}^* \cdot \nabla)\, \mathbf{m} + \sum_{F \in \mathcal{F}_h^{\mathrm{i}}} \int_F [\![\mathbf{v}]\!] \cdot \mathbf{H}_{\mathrm{LF}}\left(\mathbf{u}^*, \mathbf{m}\right), \tag{8}$$

where $\mathbf{u}^*$ is the convective field and $\mathbf{H}_{\mathrm{LF}}$ the Lax-Friedrichs flux function:

$$\mathbf{H}_{\mathrm{LF}}\left(\mathbf{u}^*, \mathbf{m}\right) = \frac{\alpha}{2} [\![\mathbf{m}]\!] + \mathbf{n}_{\mathrm{F}} \cdot \{\mathbf{u}^* \mathbf{m}\}, \tag{9}$$

where α is the local convection speed. No boundary terms are present, since we consider wall-bounded flows.

2.1.2. Temporal discretization and solution of linear systems

The general transport equation for quantity ξ is discretized implicitly in time with Backward Differentiation Formulae (BDF) of order M (with constant time step Δt):

$$\frac{\gamma_0}{\Delta t}\xi^{n+1} + A(\mathbf{u}^*)\xi^{n+1} = \sum_{j=1}^{M} \frac{\gamma_j}{\Delta t}\xi^{n+1-j} + S_\xi^{n+1}. \tag{10}$$

For $M = 2$, $\gamma_0 = 3/2$, $\gamma_1 = -2$, and $\gamma_2 = 1/2$. Matrix A collects all contributions deriving from the discretization of diffusive and convective terms; the latter introduces non-linearities that are solved with an M^{th}-order extrapolation of the velocity field from the previous steps: $\mathbf{u}^* = \sum_{j=1}^{M} \theta_j \mathbf{u}^{n+1-j}$. For $M = 2$, $\theta_1 = 2$ and $\theta_2 = -1$.

To solve the coupled momentum-continuity system (2)-(3), we choose the second-order time accurate pressure correction scheme described by Van Kan [8]; the splitting of the equations is done at an algebraic level, as explained in [7], to avoid the imposition of pressure boundary conditions.

In `DGFlows`, which is fully parallelized, we use METIS to partition the mesh [9] and the MPI-based software library `PETSc` [10] to assemble and solve all linear systems. The pressure-Poisson equation is solved with the conjugate gradient method and an additive Schwarz preconditioner, with one block per process and an incomplete Cholesky factorization on each block; the other equations are solved with the GMRES method and a block Jacobi preconditioner, with one block per process and an incomplete LU factorization on each block.

2.2. Neutronics: `PHANTOM-S`$_N$ Code

`PHANTOM-S`$_N$ solves the multi-group Linear Boltzmann radiation transport equation (LBE), steady-state or time-dependent. The code has extensive capabilities, such as both principal and

multi-modal calculations of various eigenvalue types (criticality and time eigenvalues) [11], both regular and generalized perturbation analysis [12], and goal-oriented spatial refinement [13]. In liquid-fueled systems, the precursors equations have to be solved for explicitly due to the transport of fission products. Therefore, the model equations read (using standard notation and omitting dependencies for clarity)

$$\frac{1}{v}\frac{\partial \varphi_g}{\partial t} + \mathbf{\Omega}\cdot\nabla\varphi_g + \Sigma_t\varphi_g = \sum_{g'}\int_{4\pi}\Sigma_{s,g'\to g}(\mathbf{\Omega}'\cdot\mathbf{\Omega})\varphi_{g'}\mathrm{d}\mathbf{\Omega}' + \frac{(1-\beta)\chi_g^p}{4\pi}\sum_g \nu\Sigma_f\Phi_g + \frac{\chi_g^d}{4\pi}\sum_g \lambda_i C_i, \tag{11}$$

$$\frac{\partial C_i}{\partial t} + \nabla\cdot(\mathbf{u}C_i) + \lambda_i C_i = \nabla\cdot(D_{eff}\nabla C_i) + \beta_i\sum_g \nu\Sigma_f\Phi_g, \tag{12}$$

with g and g' spanning all the energy groups and i the families of delayed neutron precursors. D_{eff} is an effective diffusion coefficient which can be computed as $D_{eff} = (\nu/Sc) + (\nu_t/Sc_t)$, where ν and ν_t are the molecular and turbulent kinematic viscosities, while Sc and $Sc_t = 0.85$ the molecular and turbulent Schmidt numbers. Boundary conditions for the neutron flux equation are standard reflective and void. For wall-bounded flows, in absence on any inflow, the only boundary condition for C_i is no diffusive flux ($\mathbf{n}\cdot\nabla C_i = 0$)

2.2.1. Spatial and temporal discretizations and solution of the linear systems

Discretization of Eq. (11) is done by the discrete ordinates method in angle and by the DG-FEM in space. We refer to [14] for the standard approach. The diffusive and convective terms present in Eq. (12) are discretized as described in Section 2.1.1. Both equations are implicitly discretized in time adopting the BDF schemes described in Section 2.1.2. The resulting linear system can be cast into the following block form:

$$\begin{pmatrix} A_\varphi & \Lambda \\ F & A_C(\mathbf{u}^*) \end{pmatrix}\begin{pmatrix}\varphi \\ C\end{pmatrix}^{n+1} = \begin{pmatrix} b_\varphi \\ b_C\end{pmatrix}, \tag{13}$$

where A_φ represents the discretization of the multi-group LBE, Λ the precursor decay in the LBE, $A_C(\mathbf{u}^*)$ the precursors convection, diffusion, and decay, and F is the precursor fission production block. In PHANTOM-S_N, the coupled system is solved by an asymmetric Krylov method (e.g., BiCGSTAB), with a physics-based preconditioning approach, where flux and precursor equations are solved by a block Gauss-Seidel method. Precursors subsystems are solved with GMRES and ILU preconditioner implemented in PETSc. The multi-group flux subsystem is solved with Gauss-Seidel iterations (or a Krylov method with a Gauss-Seidel preconditioner), and the group fixed source problems are solved with a Krylov method preconditioned with a directional sweep procedure; convergence of source iteration is enhanced by diffusion synthetic acceleration in highly scattering media. We refer to [11] for more details about the solution of the multi-group problem.

2.3. Coupling Strategy and Cross Sections Treatment

Figure 2 displays the structure of the multi-physics code . In transient simulations, a loose-coupling strategy is adopted, where PHANTOM-S_N is called first and, after completion of a time-step, DGFlows is called to handle the flow physics. Several data are exchanged between the codes, once per time step: velocity and turbulent viscosity fields influence the precursors distribution, so

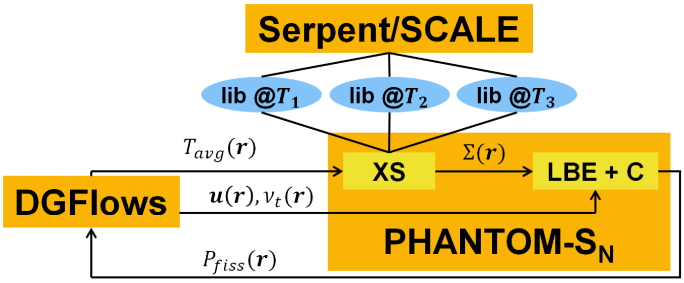

Figure 2: Structure of the multi-physics code.

they are exported from `DGFlows` to `PHANTOM-`S_N; fission power density is part of the energy source in Eq. (1), so it follows the inverse route. `DGFlows` computes an average temperature on each element and exports it to the routines in `PHANTOM-`S_N devoted to the computation of cross sections. Based on these temperatures, cross sections to be used in the LBE and in the precursors equations are interpolated starting from a set of libraries at prescribed temperatures, generated by Serpent or SCALE. In case only one library is prescribed, cross sections are corrected with density and Doppler feedback, according to

$$\Sigma_r(T) = \left[\Sigma_r(T_0) + \alpha_r \log\left(\frac{T}{T_0}\right)\right] \frac{\rho(T)}{\rho_{ref}}, \tag{14}$$

where T_0 is the library reference temperature, which the Doppler coefficients α_r are calculated at. In steady-state simulations, the codes are iterated until sufficient convergence.

2.4. Meshes generation and handling

Both codes can handle structured or unstructured meshes with tetrahedra or hexahedra elements (triangles or quadrangles in 2D), created with the open source tool `Gmsh` [15]. Starting from the same "master" mesh, each code independently can perform a local, hierarchical refinement where needed (e.g., near wall regions in `DGFlows`). This makes exchange of data easy through Galerkin projection.

3. CODE VERIFICATION: THE CNRS BENCHMARK

Validation and verification of multi-physics codes for fast-spectrum MSRs is a challenging task, given the lack of experimental data. Here, we present the results obtained performing the purpose-made numerical benchmark developed at LPSC/CNRS/Grenoble [4,16]. Its goal is to test the physics coupling capabilities of code systems, focusing on the specific features of the MSFR: fast spectrum, strong density feedback, precursor drift. It adopts a step-by-step approach: (1) single physics with only one-way coupling, (2) full coupling at steady-state, and (3) transient coupling, in order to identify sources of discrepancy in the coupling of different physics. Sources of complexity as 3D geometry, turbulent flow, and Doppler feedback are avoided.

Figure 3 depicts the domain of the problem: a 2 m x 2 m insulated cavity, surrounded by vacuum, filled with molten salt at initial temperature of 900 K. A zero-velocity boundary condition

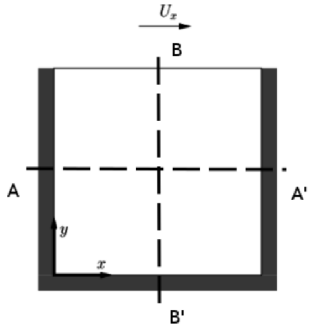

Figure 3: CNRS benchmark: 2 m x 2 m cavity domain. It is insulated, surrounded by vacuum, and filled with molten salt at initial temperature of 900 K [4,16].

is imposed at all walls, except the lid, which moves at U_x (varying from 0 to 0.5 ms^{-1}). Since all walls are adiabatic, salt cooling is mimicked via an artificial heat sink $S_h = h(T - T_{ext})$, where $T_{ext} = 900$ K and the volumetric heat transfer coefficient h is uniform and equal to 10^6 WK^{-1}m^{-2}. Buoyancy effects are modeled through the Boussinesq approximation; all fluid properties are constant in space and temperature independent. Neutron precursors are divided in 8 families, while cross sections are provided for a 6-groups discretization; the latter are computed at the reference temperature of 900 K and corrected only with the density feedback. Reactor power is normalized to P, varying up to 1.0 GW (the steady-state steps are, in fact, criticality eigenvalue problems). We refer to [4,16] for a complete description of the benchmark, as well as details regarding fuel salt composition and thermophysical properties, cross-sections, and precursors fractions and decay constants.

We discretized the domain into a 50x50 uniform structured mesh, without any local refinement, approximating the velocity with polynomial order $\mathcal{P}= 2$ and all other quantities with $\mathcal{P}= 1$. These options proved to ensure mesh-independent results. Since scattering cross sections were provided up to order P_3, we compared the results obtained with an S_2 discretization, qualitatively close to diffusion, and with a "full-transport" S_6 one.

We present the results obtained for Step 1.5 of the benchmark: the fully-coupled, steady-state solution is sought for $P = 1$ GW and $U_x = 0$, thus testing the code's capabilities to reproduce the effects of the natural convection induced by fission source. Figure 4 shows the velocity and temperature fields obtained, together with the distributions of precursors belonging to a long-lived and a short-lived family. They are in very good agreement with those reported in [4]. Table 1 reports the reactivity change with respect to the isothermal, static case for different values of P. As expected, higher power levels correspond to higher values of $\Delta\rho$, due to the increased maximum temperature in the system; in fact, higher temperatures enhance salt expansion and buoyancy, whose effect is to drive neutron precursors from the cavity center to regions of lower neutron importance. Agreement with the values reported in [4] is good: for the maximum power case, a maximum difference of 57.1 pcm is denoted for the S_2 discretization and of 80.7 pcm for the S_6 one. In relative terms, the maximum mismatch is of 6.5% for the S_2 discretization and of 8.4% for the S_6 one ($P = 0.4$ GW case). This discrepancy is considered satisfactory taken into account the differences in neutronics models (Transient Fission Matrix approach in [4]) and in

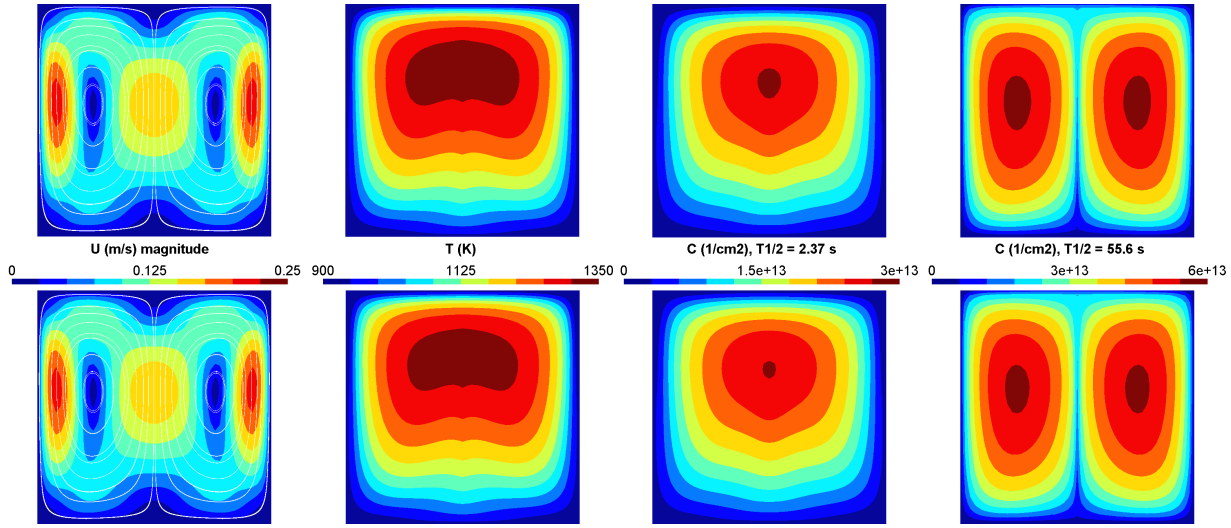

Figure 4: CNRS benchmark: fields obtained in Step 1.5 for S_2 (top) and S_6 (bottom) discretizations. From left to right: velocity magnitude with streamlines (seeds sampled uniformly along the AA' line), temperature, short-lived and long-lived precursors.

Table 1: CNRS benchmark: Comparison of $\Delta\rho$ obtained in the steady-state coupled step.

$\rho - \rho_{stat}$ **(pcm)**					
Codes	**Power (GW)**				
	0.2	0.4	0.6	0.8	1.0
TUD-S_2	-263.7	-498.1	-731.1	-967.2	-1208.5
TUD-S_6	-258.0	-487.8	-716.3	-947.9	-1184.4
CNRS-TFM [4]	-278.3	-533.1	-780.7	-1024.3	-1265.2

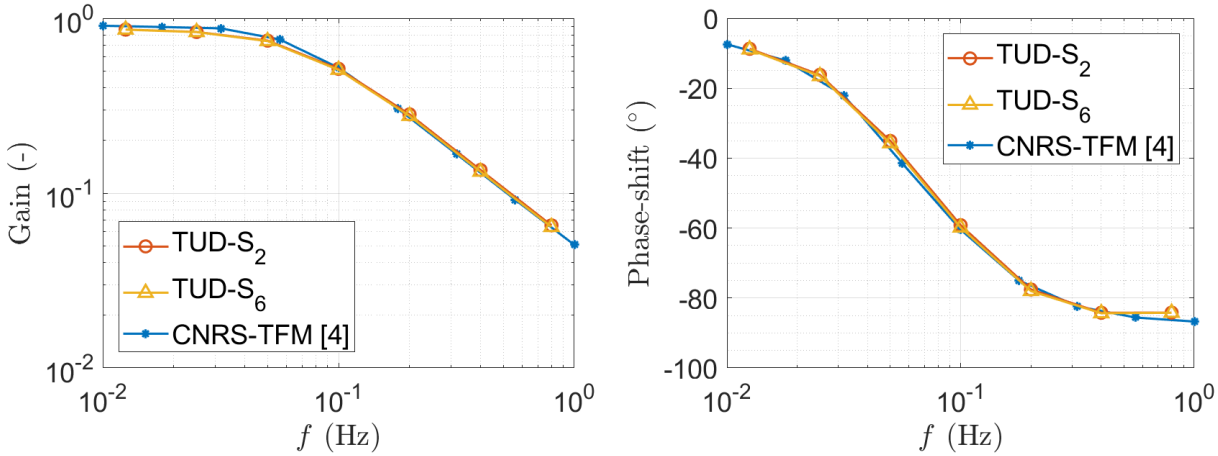

Figure 5: CNRS benchmark: Comparison of Bode diagrams obtained in the transient coupled step.

cross sections correction approaches (point-wise in [4]).

Finally, we show the results obtained for Step 2 of the benchmark, which tests the code's capabilities to capture the system response, in terms of gain and phase shift, to (small) perturbations in the entire frequency space. Starting from the fully coupled stationary solution at $P = 1$ GW and $U_x = 1$ ms^{-1}, the volumetric heat transfer coefficient h is varied according to a sine wave of frequency $f \in [0.0125, 0.025, 0.05, 0.1, 0.2, 0.4, 0.8]$ Hz; the perturbation in the salt cooling leads to a sinusoidal power trend induced by the negative density feedback coefficient. Figure 5 shows the Bode diagrams of power gain and phase-shift we obtained, evaluated when the system reached an asymptotic, periodic response after each perturbation. We chose the BDF2 scheme for temporal discretization and a time step equal to $1/200$ of the h-wave period. As expected, at low frequencies, precursors can find an equilibrium at each instant, so the power follows the extracted one (gain ≈ 1 and minimal phase-shift). At high frequencies, on the contrary, fast neutrons govern the kinetics (due to the long precursors half-lives), but they cannot sustain the chain reaction, so there is a reduction in the system response amplitude and the phase shift gets close to $-90°$. Our results are in excellent agreement with those reported in [4] (for different frequencies), with differences limited to 5% for the gain and 4% for the phase-shifts.

4. CONCLUSIONS

This paper has presented a novel multi-physics code for liquid fueled fast reactors being developed at TU Delft. A loose-coupling is realized between an S_N radiation transport code and a RANS solver. Both tools are based on the Discontinuous Galerkin FEM for space discretization, whose advantages guarantee high accuracy of simulations, and implicit BDF time discretization.

In the absence of more realistic experimental data, the multi-physics tool was benchmarked against a suitable numerical problem created at LPSC/CNRS/Grenoble. Excellent agreement is found with results present in literature. Differences are limited to a few percent maximum, and are mainly due to the different approach we adopt for correcting cross sections with the temperature. In conclusion, the benchmark proved that the multi-physics tool is able to reproduce accurately both the stationary and dynamic behavior of fast liquid fuel systems, with all their unique physics phenomena. Therefore, the code can be used to simulate transient scenarios in the MSFR, to assess the safety of the current design. For this purpose, the benefits of a more tight coupling between the codes will be investigated.

ACKNOWLEDGMENTS

This project has received funding from the Euratom research and training programme 2014-2018 under grant agreement No 661891. The authors would like to thank Dr. M. Aufiero, Dr. P. Rubiolo, and Dr. A. Laureau for providing all the necessary data to perform the benchmark described in Section 3.

REFERENCES

[1] D. LeBlanc. "Molten salt reactors: A new beginning for an old idea." *Nuclear Engineering and Design*, **volume 240**, pp. 1644–1656 (2010).

[2] M. Allibert, M. Aufiero, M. Brovchenko, S. Delpech, V. Ghetta, D. Heuer, A. Laureau, and E. Merle-Lucotte. "Molten salt fast reactors." In I. L. Pioro, editor, *Handbook of Generation IV Nuclear Reactors*, pp. 157–188. Woodhead Publishing (2016).

[3] C. Fiorina, D. Lathouwers, M. Aufiero, A. Cammi, C. Guerrieri, J. L. Kloosterman, L. Luzzi, and M. E. Ricotti. "Modelling and analysis of the MSFR transient behaviour." *Annals of Nuclear Energy*, **volume 64**, pp. 485–498 (2014).

[4] A. Laureau. *Développement de modèles neutroniques pour le couplage thermohydraulique du MSFR et le calcul de paramètres cinétiques effectifs*. Ph.D. thesis, Grenoble Alpes University, France (2015).

[5] M. Aufiero, P. Rubiolo, and M. Fratoni. "Monte Carlo/CFD coupling for accurate modeling of the delayed neutron precursors and compressibility effects in molten salt reactors." In *Transactions of the American Nuclear Society*, volume 116, pp. 1183–1186. San Francisco, California (2017).

[6] E. Cervi, S. Lorenzi, A. Cammi, and L. Luzzi. "Development of a multiphysics model for the study of fuel compressibility effects in the Molten Salt Fast Reactor." *Chemical Engineering Science*, **volume 193**, pp. 379–393 (2019).

[7] K. Shahbazi, P. F. Fischer, and C. R. Ethier. "A high-order discontinuous Galerkin method for the unsteady incompressible Navier–Stokes equations." *Journal of Computational Physics*, **volume 222**, pp. 391–407 (2007).

[8] J. van Kan. "A second-order accurate pressure correction scheme for viscous incompressible flow." *SIAM Journal on Scientific and Statistical Computing*, **volume 7**, pp. 870–891 (1986).

[9] G. Karypis and V. Kumar. "A Fast and High Quality Multilevel Scheme for Partitioning Irregular Graphs." *SIAM Journal on Scientific Computing*, **volume 20**, pp. 359–392 (1998).

[10] S. Balay, S. Abhyankar, M. F. Adams, J. Brown, P. Brune, K. Buschelman, L. Dalcin, A. Dener, V. Eijkhout, W. D. Gropp, D. Kaushik, M. G. Knepley, D. A. May, L. Curfman McInnes, R. Tran Mills, T. Munson, K. Rupp, P. Sanan, B. F. Smith, S. Zampini, H. Zhang, and H. Zhang. "PETSc Users Manual." Technical Report ANL-95/11 - Revision 3.10, Argonne National Laboratory (2018).

[11] J. Kópházi and D. Lathouwers. "Three-dimensional transport calculation of multiple alpha modes in subcritical systems." *Annals of Nuclear Energy*, **volume 50**, pp. 167–174 (2012).

[12] Z. Perkó, D. Lathouwers, J. L. Kloosterman, and T. van der Hagen. "Adjoint-Based Sensitivity Analysis of Coupled Criticality Problems." *Nuclear Science and Engineering*, **volume 173**, pp. 118–138 (2013).

[13] D. Lathouwers. "Goal-oriented spatial adaptivity for the S_N equations on unstructured triangular meshes." *Annals of Nuclear Energy*, **volume 38**, pp. 1373–1381 (2011).

[14] T. A. Wareing, J. M. McGhee, J. E. Morel, and S. D. Pautz. "Discontinuous Finite Element S_N Methods on Three-Dimensional Unstructured Grids." *Nuclear Science and Engineering*, **volume 138**, pp. 256–268 (2001).

[15] C. Geuzaine and J. Remacle. "Gmsh: A 3-D finite element mesh generator with built-in pre- and post-processing facilities." *International Journal for Numerical Methods in Engineering*, **volume 79**, pp. 1309–1331 (2009).

[16] M. Aufiero and P. Rubiolo. "Testing and verification of multiphysics tools for fast-spectrum MSRs: the CNRS benchmark." In *International Seminar on Nuclear Reactor Core Thermal Hydraulics Analysis (IS-ReCTHA 2018)*. Lecco (2018).